2

X-601-72-489
PREPRINT

NASA TM X- 70433

AN EMPIRICAL MODEL OF ENERGETIC SOLAR PROTON FLUXES WITH APPLICATIONS TO EARTH ORBITING SPACECRAFT

E. G. STASSINOPOULOS
J. H. KING

DECEMBER 1972

GSFC — GODDARD SPACE FLIGHT CENTER —
GREENBELT, MARYLAND

Reproduced by
NATIONAL TECHNICAL
INFORMATION SERVICE
US Department of Commerce
Springfield, VA. 22151

N73-30769

(NASA-TM-X-70433) AN EMPIRICAL MODEL OF ENERGETIC SOLAR PROTON FLUXES WITH APPLICATIONS TO EARTH ORBITING SPACECRAFT (NASA) 33 p HC $3.75 CSCL 03B

G3/29 Unclas 12454

33

An Empirical Model of Energetic Solar Proton Fluxes with Applications to Earth Orbiting Spacecraft

E. G. Stassinopoulos

and

J. H. King

December 1972

NASA - GODDARD SPACE FLIGHT CENTER

Greenbelt, Maryland

CONTENTS

SUMMARY

An empirical model for energetic solar proton fluxes is presented. With this model, the effects of such protons on geocentric space missions, to be flown during the next solar active period (1966-1983) and with orbits involving partial magnetospheric shielding, may be estimated.

A synoptic background review is given, followed by a detailed discussion of the model's analytic development. Also given are comments on the model's use, errors, uncertainties, and limitations, including sample calculations which demonstrate the application of specific or general project missions. Finally, for circular trajectories, percentage exposure maps are presented, depicting fractional mission times spent outside particular L-shells as functions of orbit altitude and inclination.

The distinguishing assumptions of this analysis are: (1) that the solar proton flux in the 10-100 Mev energy range, as accumulated over solar cycle 20 due to several discrete solar events, will be accumulated at a uniform rate for the seven active years of solar cycle 21, and (2) that all protons in the energy range of interest have a common geomagnetic latitude cutoff.

INTRODUCTION

The purpose of this note is to describe the interplanetary proton fluxes of solar origin observed at 1 A.U. between the years 1964 and 1972 for integral threshold energies at 10, 30, and 60 Mev, and to introduce a method for obtaining practical approximations to these fluxes as a function of energy and time.

In the past, workers in applied study areas such as satellite design, component development, or mission planning, often used either estimates of expected energetic solar proton fluxes derived from cycle 19 ground observations or used approximations based on fractional cycle 20 data usually obtained from a single independent source without comprehensive temporal or spectral coverage.

The present study proposes a more representative empirical solar proton model for the energy range 10-100 Mev, derived entirely from cycle 20 experimental measurements and based on a uniform, coherent, and homogeneous treatment of several available data sets. A description of its development, from an analysis and evaluation of the data, is given in following sections.

Throughout this work one overriding consideration prevailed: to produce a versatile, simple, and practical model that would be easy to use while yielding results within acceptable error limits. In view of this scope, some simplifying assumptions were made along the way in order to reduce the complexity of the problem.

Crude confidence levels, that is, the probability of actual cycle 21 fluxes exceeding the predicted intensities, are included in this effort. A formal statistical treatment will be found in King (1973), where the probability of exceeding given mission fluence levels is calculated as a function of mission duration and energy.

PHYSICAL BACKGROUND

A. The Media

Due to the inability of the solar gravitational field to contain its extremely hot corona, the coronal plasma expands radially away from the sun and draws out the coronal magnetic field in the process. The resultant transsonic flow is referred to as the solar wind, and extends past the earth to a distance of several tens of astronomical units (1 A.U. = earth-sun separation distance).

As the result of diamagnetic effects, the geomagnetic field causes a cavity to be formed in the solar wind. Conversely, the geomagnetic field, which would extend to infinity in the absence of current systems external to the earth, is confined to a finite region of space by the solar wind. The geomagnetic cavity in the solar wind, called the magnetosphere, is approximately hemispherical on the day side of the earth with a boundary at about 10 to 12 earth radii geocentric distance. On the night side the sweeping action of the solar wind results in the formation of the geomagnetic tail which is approximately cylindrical in shape, antisolar in direction, several hundred earth radii in length, and about forty earth radii in diameter.

The regions of space occupied by the solar wind and by the earth's magnetosphere are referred to as interplanetary and magnetospheric. Cislunar interplanetary space is that region of interplanetary space in the immediate vicinity of the earth-moon system.

B. The Particles

Interplanetary energetic particle populations are of two sources. Galactic particles (as observed in cislunar space) that have spectra which are peaked in the 0.5 - 1.0 Gev range and which vary with an 11 year periodicity corresponding to different levels of modulation by the interplanetary extension of solar magnetic fields. In the energy range of interest in this paper, yearly-averaged galactic fluxes are not further considered in this note, but are discussed in detail in Burrell and Wright (1972).

Solar particles, which in the energy regime of interest result from acceleration in solar flares by process not yet well understood. Particles accelerated in flares include electrons, protons, alpha particles, and heavier nuclei. Fluxes of heavier nuclei are very small relative to proton fluxes, and probably pose no hazard to space systems. Electrons, due to their very small masses, likewise cause little damage. Alpha particle fluxes typically amount to 2-10% of the proton fluxes for similar energies and could on occasion be troublesome. However, due to the diminished abundance and importance of alpha particle data relative to the available proton data, this discussion will be restricted to solar proton

fluxes only.

Because propagation of solar protons is controlled by the plasma and the magnetic fields in the lower corona and in interplanetary space, particle flux profiles observed by interplanetary spacecraft are often very complex. Typically, particle onset begins several tens of minutes to several hours after the parent flare; peak flux usually occurs between two hours and one day after the flare; fluxes usually decay to background within a few days to one week after the flare. There is a tendency for particle-producing flares to occur in groups, so that very often flare-associated flux enhancements may occur well before the particle flux of a previous flare has decayed to background, even though appreciable time intervals (weeks-months) may occur during which no solar event is observed.

Solar particle fluxes in the magnetosphere are more complex than interplanetary fluxes because the earth's magnetic field prevents low energy solar particles from penetrating deeply into the magnetosphere, except near the magnetic poles. Thus, protons with energies below a given value are excluded from a shell of dipolar magnetic field lines intersecting the northern and southern hemispheres along a corresponding constant geomagnetic "cutoff" latitude. Only protons with increasingly higher energies are able to penetrate deeper into the magnetosphere and reach correspondingly lower magnetic latitudes. In order to describe the magnetospheric access to solar protons, the specification of this

For the particles considered in this study, that is protons in the energy range 10-100 Mev, the cutoff latitudes lie between 60° and 70°. A diurnal variation of 2° to 4° has been observed, presumably associated with geomagnetic tail effects and apparently affecting all energies. Variations of similar or somewhat larger amplitudes also occur, that are associated with geomagnetic storms. The magnitude of such storm induced changes in cutoff latitude varies with each event, depending on flare heliolongitude and flare frequency.

Due to these variations, and due to the fact that this analysis is intended to be used for temporal extrapolations into the next solar cycle which have a significant intrinsic uncertainty, we have chosen to describe solar proton entry into the magnetosphere in terms of a highly simplified picture. It was assumed that protons of all energies above 10 Mev have free access to all magnetospheric regions external to a shell characterized by dipole field lines intersecting the globe at a geomagnetic latitude of 63°, and have no access to the remainder of the magnetosphere. In the magnetic equatorial plane this corresponds to free access to 5 earth radii geocentric distance. Note that this assumption results in a somewhat softer orbit-integrated spectrum that would be obtained from a rigidity-dependent cutoff analysis.

A good review of magnetospheric cosmic ray cutoffs and their variations is given by Lanzerotti (1972), while Fanselow and Stone (1972), and references therein, present more current observational data.

C. The Observations

The most continuous set of data covering solar proton fluxes during the twentieth solar cycle (1964-1975) is that available from the IMP series of spacecraft launched into highly elliptical geocentric trajectories. These interplanetary observations are used to generate a list of peak and event-integrated fluxes for the major recorded proton events. From that list, yearly solar proton fluxes are then obtained, which in turn are used in the ensuing analysis.

The first list includes

(a) the only significant cycle-20 event that occurred prior to the launch of IMP 3,

(b) all events that occurred during the life of IMP 3 (May 1965 to May 1967) in which the peak flux of protons above 20 Mev was greater than 1 $(cm^2\text{-ster-sec})^{-1}$, according to the GSFC data (as taken from Kinsey, 1969), and

(c) all events that occurred during the lives of IMPs 4 and 5 (May 1967 to present) in which the peak flux of protons above 10 Mev was greater than 25 $(cm^2\text{-ster-sec})^{-1}$, according to the data of C.O. Bostrom (Johns Hopkins University/Applied Physics Lab) published monthly by NOAA in Solar-Geophysical Data.

Note that the criteria used for selecting events in (b) and (c) are mutually consistent for an integral power law energy spectrum characterized by the exponent -4.65.

All fluxes were taken to be isotropic in obtaining this list and in the subsequent analysis. On an event-integrated basis, departures from isotropy are typically only a few percent or less. This applies to the interplanetary medium and to much of the magnetosphere, but may not apply at low altitudes where anisotropy should result from atmospheric loss mechanisms.

Table A contains the data for the events that occurred before the launch of IMP 4. Table B contains data for events that occurred after the launch of IMP 4. Peak fluxes (Jpk) are taken directly from the Bostrom data published in Solar Geophysical Data (with subtraction of galactic background). For the period May 1967 to April 1969, integral fluxes (J_i) are computed from the best fit differential spectra obtained from GSFC (McDonald). University of Chicago (Simpson), Bell Laboratories (Lanzerotti), and JHU/APL Bostrom data. The fits themselves are given in Table 3 of the King, 1972 report. For the period of November 1969 to November 1970, the integral fluxes are as computed from the estimated curves that best fit GSFC and JHU/APL data. For the 1971 to 1972 time period, the integral fluxes represent JHU/APL data only.

From the data of Tables A and B, Figure 1 was generated. It illustrates the annual integrated fluxes of protons above 10, 30, and 60 Mev for the 1964-1972 time period. It is immediately apparent that except for 1970, the annual fluxes were approximately constant over the six year interval 1966-1971. For earlier years, the fluxes are negligible relative to the active years (and also to the galactic fluxes). For 1972, owing to the August events, the annual fluxes are significantly larger than those for earlier years. In fact, the 1972 annual flux of protons above 10 Mev is greater by a factor of 2 than the corresponding flux as summed over 1964 through 1971. At 30 and 60 Mev, this factor is more nearly 4. That such a large portion of the cycle 20 flux should have occurred during only one week of the eleven year cycle, dramatically illustrates the difficulty of predicting solar particle fluxes to be encountered during a planned future mission. This point will subsequently be raised again.

Finally, Figure 1 shows the total proton fluxes above the three energies, summed over the entire 20th solar cycle, for all major recorded events. It is assumed that contributions to these fluxes from the remaining years of declining activity of this cycle will be negligible.

THE MODEL

A. Development

Having presented the cycle 20 solar proton data in terms of (a) event integrated fluxes for all major events, (b) yearly integrated fluxes, and (c) cycle integrated fluxes, it remains to set forth a model which may be used in predicting fluxes to be encountered by space missions of specified duration and trajectory characteristics, to be flown at specified phases into the next solar cycle.

In attempting to construct such a model, two important items have to be kept in mind. First, there is no assurance that the overall flux levels observed during the 20th solar cycle will occur during the 21st cycle. Second, there is no reliable way of predicting the distribution of individual solar events in time, in flux level, and in spectra through the 21st cycle.

With due consideration to these uncertainties, the solar cycle integrated fluxes in Figure 1 were then examined to find the best spectral representation for the data, as indicated in Figure 2. This turned out to be our exponential in rigidity* representation, specifically:

$$J(>R) = 1.5 \times 10^{11} e^{-R/88} \qquad (1)$$

*Rigidity may be thought of as a measure of the resistance of a charged particle to the bending of its trajectory by a magnetic field. For sub-relativistic protons, regidity R may be related to kinetic energy E by the expression $R = 43.3E^{\frac{1}{2}}$, with R in Mv (million volts) and E in Mev.

with J in cm^{-2} and R in Mv. The numerical values give the fit indicated in Figure 2.

For the convenience of those readers who may be more accustomed to energy than rigidity, the energy-ridigity relationship was used to express the solar cycle integrated fluxes as:

$$J(>E) = 1.5 \times 10^{11} e^{-(E/4)^{1/2}} \qquad (2)$$

where J is in units of cm^{-2} and E is in Mev.

This expression is valid over the energy range of the data, that is 10-60 Mev; but in the remainder of the analysis it will be used with the assumption, that its validity extends out to the subrelativistic energy of 100 Mev. It is not advisable to extrapolate equation 2 beyond the 10-100 Mev threshold energy range.

For simplicity, it will be assumed that the total 20th cycle fluxes were evenly accumulated over a seven year period, forming a plateau of constant amplitude extending from 1966 to 1972, henceforth called the "active" years of the cycle, without any contributions deriving from the remaining years of decreased activity.

Accordingly, one seventh of the cycle integrated fluxes may be regarded as an annual mean for its active years. This average annual intensity may then be used to estimate the expected solar proton fluxes on earth orbiting satellites during the active years of the next solar

cycle. Subsequently, the term "model" or "model flux" shall refer to this annual mean.

As a crude estimate of the confidence one may place in such a model, note that if the cycle 20 integrated flux consisted of 6 arbitrary fluence units contributed by 6 equal-amplitude events occurring during a six year solar-active period, this model would predict that future extramagnetospheric solar-active period missions of 1, 2, and 6 years would encounter 1, 2, and 6 flux units respectively. However, the statistical analysis of Burrell (1971) indicates that the probability of exceeding 1, 2, and 6 flux units on these missions is 33%, 42%, and 50% respectively. Thus, one may be more confident in the present analysis for shorter missions. Figure 3 shows the probability as a continuous function of mission duration. A more probabilistic analysis of solar cycle 20 fluxes is in preparation (King, 1973).

B. Application

The approximate number of solar particles encountered by a satellite during a given mission depends on the amount of time spent by the spacecraft outside the geomagnetic cavity, in cislunar space, plus the amount of time spent within the accessible (to these particles) regions of the magnetosphere. The sum of these times determines the true exposure time which is a characteristic of that particular mission.

Evaluated for the entire mission duration in units of years, the total exposure time becomes a proportionality factor between satellite incident fluxes and model fluxes, provided the latter are given in units of annual intensities.

For most near-earth space missions however, it is not necessary to perform lengthy computer calculations covering the entire operational lifetime of a satellite in order to evaluate the exposure factor. Very good approximations can be obtained from relatively short flight simulations (or real flight data considerations). Thus, for circular trajectories, depending on their altitude and/or inclination, about 15 to 30 revolutions (periods) are sufficient to determine the fractional exposure time for the mission. The correct proportionality factor is then the ratio of this exposure time to the interval of its evaluation. The total flux encountered is then obtained by multiplying the model flux by this ratio. Elliptical trajectories require longer flight time intervals, frequently up to several days or weeks, depending on eccentricity, perigee and apogee altitude, and inclination.

Since all solar protons in the energy range of interest were assumed (section 2-B) to have one common cut-off latitude, the characteristic exposure time of a given trajectory must consequently be the same for all energies considered. Hence, the calculated exposure factor may be indiscriminately applied to the entire model spectrum.

C. Discussion

1. Exposure Maps

For geocentric missions with circular trajectories, percentage exposure maps were constructed as functions of orbit altitude and inclination. These maps depict "isopercentage exposure contours", representing as a percentage rate the amount of mission time spent by a satellite in regions of space that are external to given dipole cutoff shells. Figures 4-6 are such geomagnetic exposure maps, where the contours were calculated for dipole cutoff shells determined by values of the McIlwain parameter L equal to 5, 6, and 7 earth radii; in terms of invariant magnetic latitude, these cutoff values correspond to $\Lambda = 63.4$, $\Lambda = 65.9$, and $\Lambda = 67.8$ degrees, respectively. In each case, the region under the zero percent curve encompasses those orbits which are completely inaccessible to solar particles. On the other hand, the region above the hundred percent contours encompasses those orbits which experience no geomagnetic shielding, and for which unaltered interplanetary conditions prevail. The region between the zero and the hundred percent curves encompasses the orbits that experience partial geomagnetic shielding.

As would be expected, the outer boundary lines display no altitude dependence. Their position, in terms of geocentric distance is determined solely by the associated dipole cutoff shell and it is equivalent to the corresponding value of L.

All maps indicate an almost linear dependence of exposure on inclination at the very low altitudes ($h < 1000$ km), while, due to the nearly vertical nature of the magnetic field lines, exposure is very weakly dependent on height in that domain. Specifically, on the map pertaining to the dipole cutoff shell of $L = 5$, Figure 4, the inaccessible region below 1000 km reaches up to an orbit inclination of about 50 degrees, and thereafter exposure increases by an average of about 0.75% per degree. Consequently, only orbits with tilts greater than 50 degrees will encounter solar protons, and only for about 0-32% of their lifetime. Towards polar inclinations, some altitude dependence is evident, with the greatest variation occurring at $i = 90°$, where the exposure rises from approximately 26% at $h = 200$ km to approximately 32% at $h = 1000$ km.

At very high altitudes ($h > 10{,}000$ km), the exposure curves, contained in the envelope formed by the two boundary contours, converge rapidly towards a focal point at the equatorial inclinations. The incomplete focusing, that is, the apparent separation between the boundary contours at the equator, is a geomagnetic geometry effect resulting from the assymetry of the magnetic field models used and from the tilt of the dipole axis to the axis of the earth's rotation.

For $h > 1000$ km, exposure appears to depend strongly on both variables, altitude and inclination. Between 10,000 km and the outer

boundary, the exposure in the range of $i > 60°$ shows a progressively weaker inclination dependence, while the contours indicate an almost linear dependence on altitude.

The accuracy of the contours is affected by the field model used in the B-L computation, the orbit generating method employed, the flight time duration considered, and the integration stepsize applied. The uncertainty due to all these factors is less than 10%, which is small relative to the uncertainty involved in applying this model to future space missions.

2. Cutoff Dependence of Percent Exposure

When the orbital parameters of inclination and altitude are fixed for a circular trajectory, the exposure time becomes a function of cutoff latitude only. Figure 7 indicates for specific missions the percentage of time spent outside a given L shell. Such curves may be constructed for any desired mission from the percent exposure maps of Figures 4-6.

The low altitude exposure contours for both inclinations shown, display only a very small change over the range $4 \leq L \leq 7$, that is, about 7% for the 60° inclination and about 10% for the 90°.

Through the assignment of cutoff L values to each particle energy, one readily determines the percentage exposure time for particles of any given energy. Recall that the present model is based upon the assumption that all particles in the 10-100 Mev energy range have a common L cutoff. However, the reader may use another assumption, and, with the figures, estimate the (varying) exposure times to particles of differing energies. For further discussions of the relation between energy and cutoff L value, see Lanzerotti (1972) and Fanselau and Stone (1972).

3. Results

To demonstrate the use of the model, some specific missions with circular and elliptical trajectories were selected for solar proton evaluation. The missions relate to actual NASA projects, but calculations are based on pre-launch nominal trajectories. The percent exposure time in each case was detained by integrating the flight path over 24 or 48 hours, for circular or elliptical orbits respectively.

The product for the percent exposure time with the mean annual model fluxes represents then the "Annual Encountered Solar Proton Fluence" for these missions. Figure 8 shows the resulting spectral curves for three IUE (SAS-D) trajectories, one SSS, one ANS, two AE (C and D), one ERTS, and one NIMBUS.

No change is expected to appear in the structure of the different spectra because of the energy independent cutoff assumption made in the model for this energy range. The only effect of varying percent exposure times is therefore a vertical displacement of the curves, without altering their shapes.

References

Burrell, M. O., "The Risk of Solar Proton Events To Space Missions", NASA TN D-6379, June 1971.

Burrell, M. O. and J. J. Wright, "The Estimation of Galactic Cosmic Ray Penetration and Dose Rates", NASA TD D-6600, March 1972.

Fanselow, J. L., and E. C. Stone, J. Geophys. Res. 77, 3999-4009, (1972).

King, J. H., "Study of Mutual Consistency of IMP 4 Solar Proton Data", National Space Science Data Center, NSSDC 72-14, Greenbelt, Maryland, Oct. 1972.

King, J. H. to be published, 1973.

Kinsey, J. H., "A Study of Low Energy Cosmic Rays at 1 A. U.", NASA-GSFC, X-611-69-396, Greenbelt, Maryland, Sept. 1969. Ph.D. Thesis, University of Maryland.

Lanzerotti, L. J., Rev. Geophys. SP. SCI. 10, 379-392 (1972).

O'Gallagher, J. J., "The Heliocentric Longitude-Intensity Profile of 15 Mev Protons from the 5 February 1965 Solar Flare", J. Geophys. Res., 75, 1163, 1970.

Paulikas, G. A., and J. B. Blake, "Solar Proton Observations at Synchronous Altitude (ATS-1) During 1967", Aerospace Corporation Report TR-0200 (4260-20) - 2, Sept. 1968.

Webber, W. R., "An Evaluation of Solar Cosmic Ray Events During Solar Minimum", Boeing Report D2-84274-1, June 1966.

Yucker, W. R., "Statistical Analysis of Solar Cosmic Ray Proton Fluence", McDonnell Douglas MDAC Paper WD 1320, June 1970.

TABLE A. INTEGRATED PROTON FLUXES FOR LARGE SOLAR EVENTS FEBRUARY 1965 - MARCH 1967

TIME PERIOD	TIME INTEGRATED FLUX $(cm^2\text{-ster})^{-1}$	THRESHOLD ENERGY (Mev)	SOURCE
Feb. 5-8, 1965	2.0×10^6	10	Webber, 1966
	6.1×10^5	15	O'Gallagher, 1970
	3.2×10^5	40	Webber, 1966
Mar. 23-26, 1966	3.7×10^5	10	Yucker, 1970
	1.4×10^5	20	Kinsey, 1969
July 7-9, 1966	3.0×10^6	10	Yucker, 1970
	9.0×10^5	20	Kinsey, 1969
Aug. 28-31, 1966	5.5×10^6	10	Yucker, 1970
	4.3×10^5	20	Kinsey, 1969
Sept. 2-6, 1966	1.3×10^8	10	Yucker, 1970
	2.0×10^6	20	Kinsey, 1969
Jan. 28 - Feb. 8, 1967	6.4×10^7	10	Yucker, 1970
	7.6×10^6	20	Kinsey, 1969
	2.4×10^7	20	Paulikas & Blake, 1968
Mar. 12-15, 1967	2.8×10^5	20	Kinsey, 1969
	4.1×10^5	20	Paulikas & Blake, 1968

TABLE B. PEAK AND INTEGRATED PROTON FLUXES FOR LARGE SOLAR EVENTS MAY 1967 - AUGUST 1972

TIME PERIOD	J_{pk}(>10 Mev) $(cm^2\text{-ster-sec})^{-1}$	J_i(>10 Mev) $(cm^2\text{-ster})^{-1}$	J_{pk}(>30 Mev) $(cm^2\text{-ster-sec})^{-1}$	J_i(>30 Mev) $(cm^2\text{-ster})^{-1}$	J_{pk}(>60 Mev) $(cm^2\text{-ster-sec})^{-1}$	J_i(>60 Mev) $(cm^2\text{-ster})^{-1}$
May 25-26, 1967	1015	4.6×10^7	32	1.7×10^6	2.3	2.5×10^4
May 28-30, 1967	115	7.1×10^6	27	1.3×10^6	9.4	4.3×10^5
Dec. 3-6, 1967	31.5	2.2×10^6	10.5	4.6×10^5	3.8	2.5×10^5
June 9-11, 1968	354	3.3×10^7	12.4	8.9×10^5	5.4	9.0×10^4
Sept. 28 (hr 12) - Oct. 2, 1968	32	3.3×10^6	19	6.9×10^5	10.3	3.4×10^5
Oct. 4-6, 1968	36	3.6×10^6	6.3	2.6×10^5	1.1	5.0×10^4
Oct. 31 - Nov. 3, 1968	133 (10/31) 152 (11/2)	2.1×10^7	10.0 (10/31) 11.7 (11/1)	1.2×10^6	1.4 (10/31) 1.1 (11/1)	2.0×10^5
Nov. 18-21, 1968	849	9.0×10^7	404	1.7×10^7	96.0	6.2×10^6
Dec. 4-9, 1968	152	2.2×10^7	31	3.2×10^6	5.2	5.6×10^5
Feb. 25 - Mar. 1, 1969	88 (2/25) 28 (2/27)	5.0×10^6	41.5 (2/25) 9.3 (2/27)	2.1×10^6	24.3 (2/25) 3.7 (2/27)	1.3×10^6
Mar. 30 - Apr. 10, 1969	26	3.5×10^6	13	1.3×10^6	8.7	8.1×10^5
Apr. 12-17, 1969	1375	1.2×10^8	123	1.6×10^7	16.0	4.6×10^6
Nov. 2-6, 1969	1317	6.9×10^7	737	2.1×10^7	201.0	9.6×10^6
Jan. 31 - Feb. 2, 1970	24.2	2.2×10^6	6.2	2.7×10^5	1.8	7.3×10^4
Mar. 6-9, 1970	93	8.0×10^6	0.9	1.0×10^5	(NO INCREASE)	6.2×10^3
Mar. 29-31, 1970	66	4.7×10^6	20.2	1.7×10^6	6.5	9.3×10^5
July 23-25, 1970	206	6.5×10^6	0.8	5.8×10^4	(NO INCREASE)	2.9×10^3
Aug. 14-17, 1970	183	2.1×10^7	2.7	3.9×10^5	0.3	3.2×10^4
Nov. 5-8, 1970	42	7.7×10^6	1.7	2.8×10^5	0.4	3.5×10^4
Jan. 24-29, 1971	1171	1.2×10^8	408	2.7×10^7	89.4	4.7×10^6
Apr. 6-8, 1971	51	2.3×10^6	5.0	2.0×10^5	1.1	2.7×10^4
Sept. 1-5, 1971	352	3.0×10^7	162	1.3×10^7	66.5	4.4×10^6
May 28 - June 1, 1972	39	5.5×10^6	2.7	5.3×10^5	1.2	1.2×10^5
Aug. 4-7 (hr 12), 1972	86000	1.64×10^9	21000	6.2×10^8	6400	1.9×10^8
Aug. 7 (hr 12)-9, 1972	3500	1.9×10^8	384	3.0×10^7	70	4.7×10^6

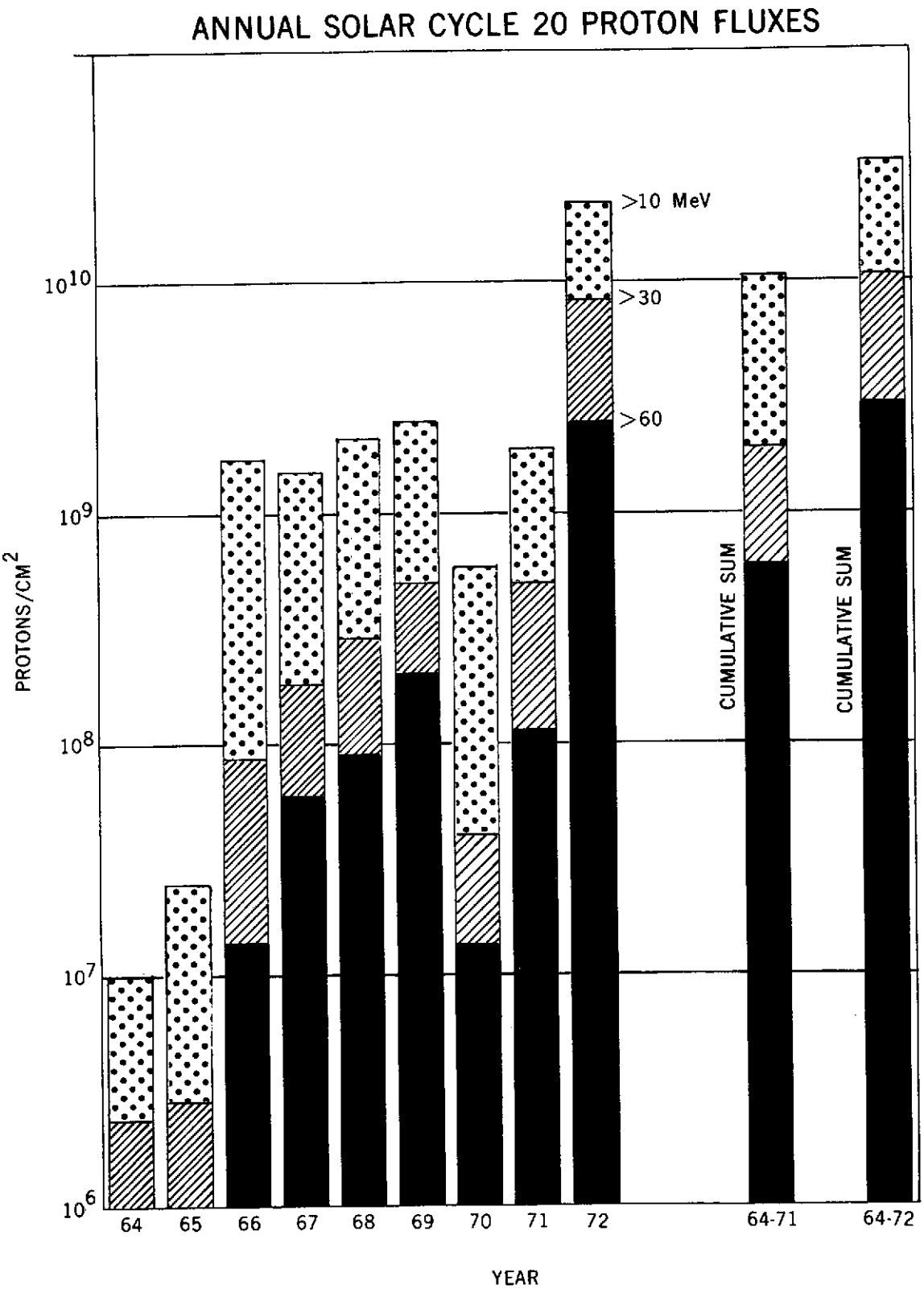
ANNUAL SOLAR CYCLE 20 PROTON FLUXES
>10 MeV
>30
>60
10^{10}
10^{9}
10^{8}
10^{7}
10^{6}
PROTONS/CM^2
CUMULATIVE SUM
CUMULATIVE SUM
64
65
66
67
68
69
70
71
72
64-71
64-72
YEAR

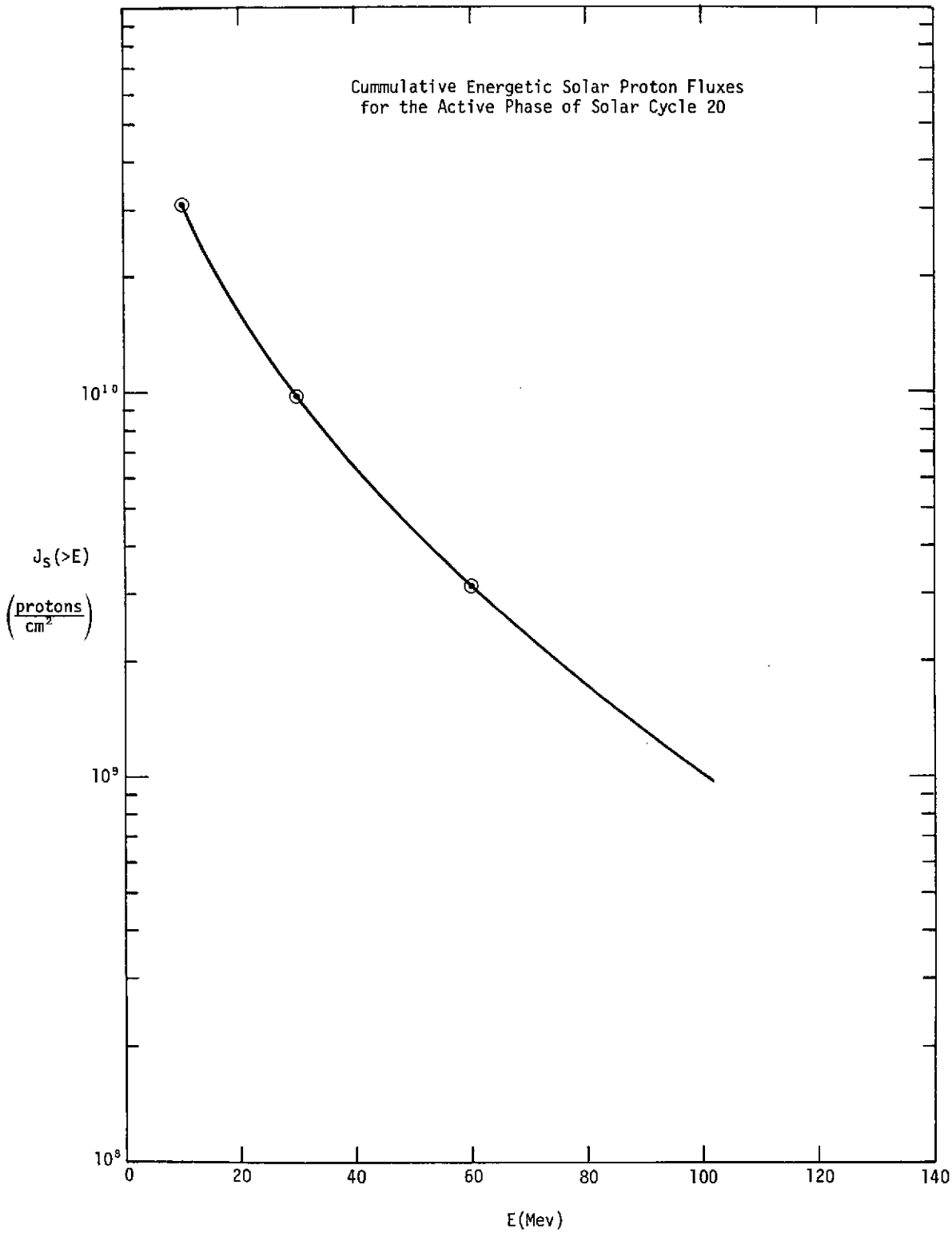
Cummulative Energetic Solar Proton Fluxes
for the Active Phase of Solar Cycle 20
$J_S(>E)$
$\left(\frac{\text{protons}}{\text{cm}^2}\right)$
10^{10}
10^9
10^8
0
20
40
60
80
100
120
140
E(Mev)

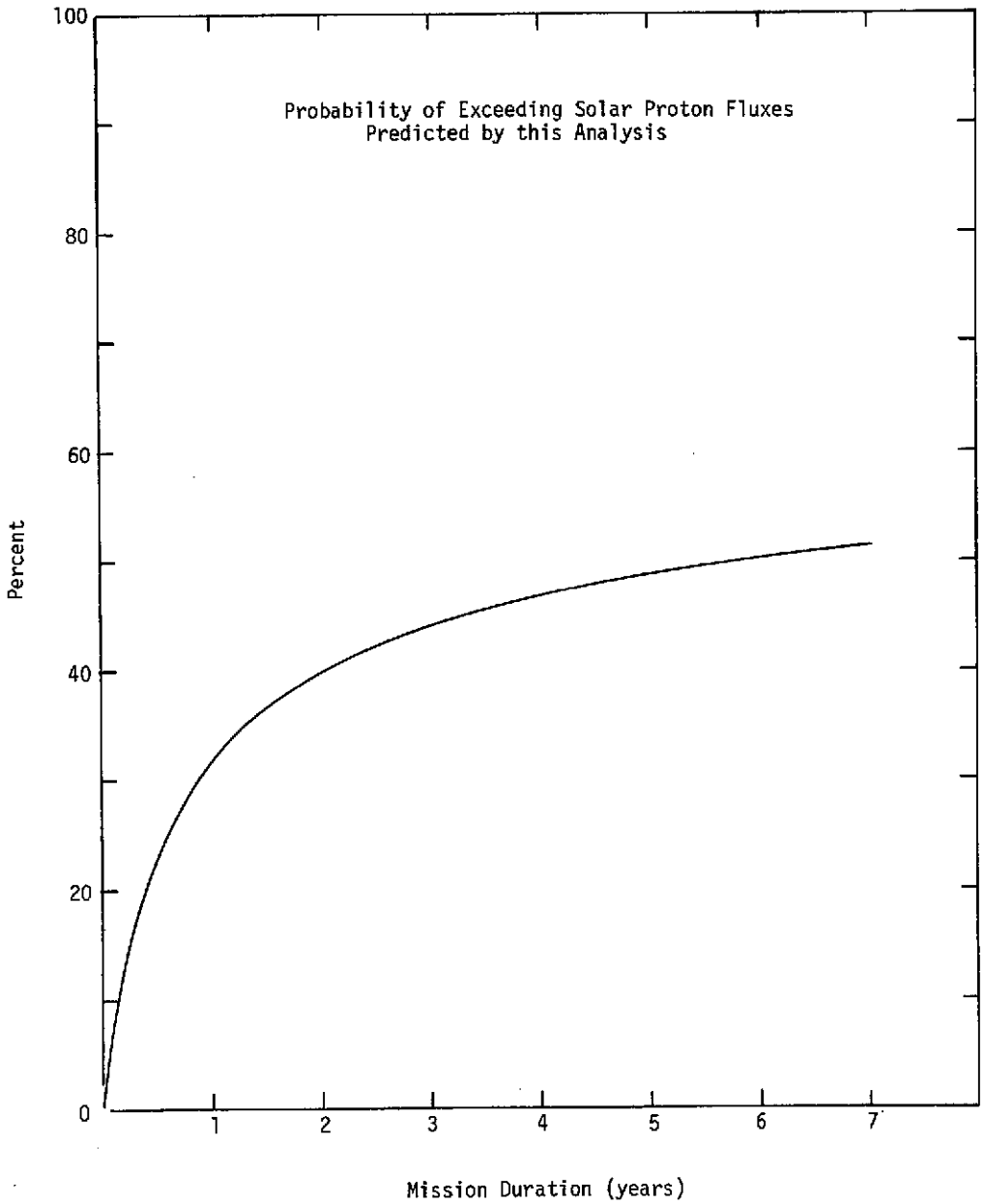
Probability of Exceeding Solar Proton Fluxes
Predicted by this Analysis
100
80
60
40
20
0
Percent
1
2
3
4
5
6
7
Mission Duration (years)

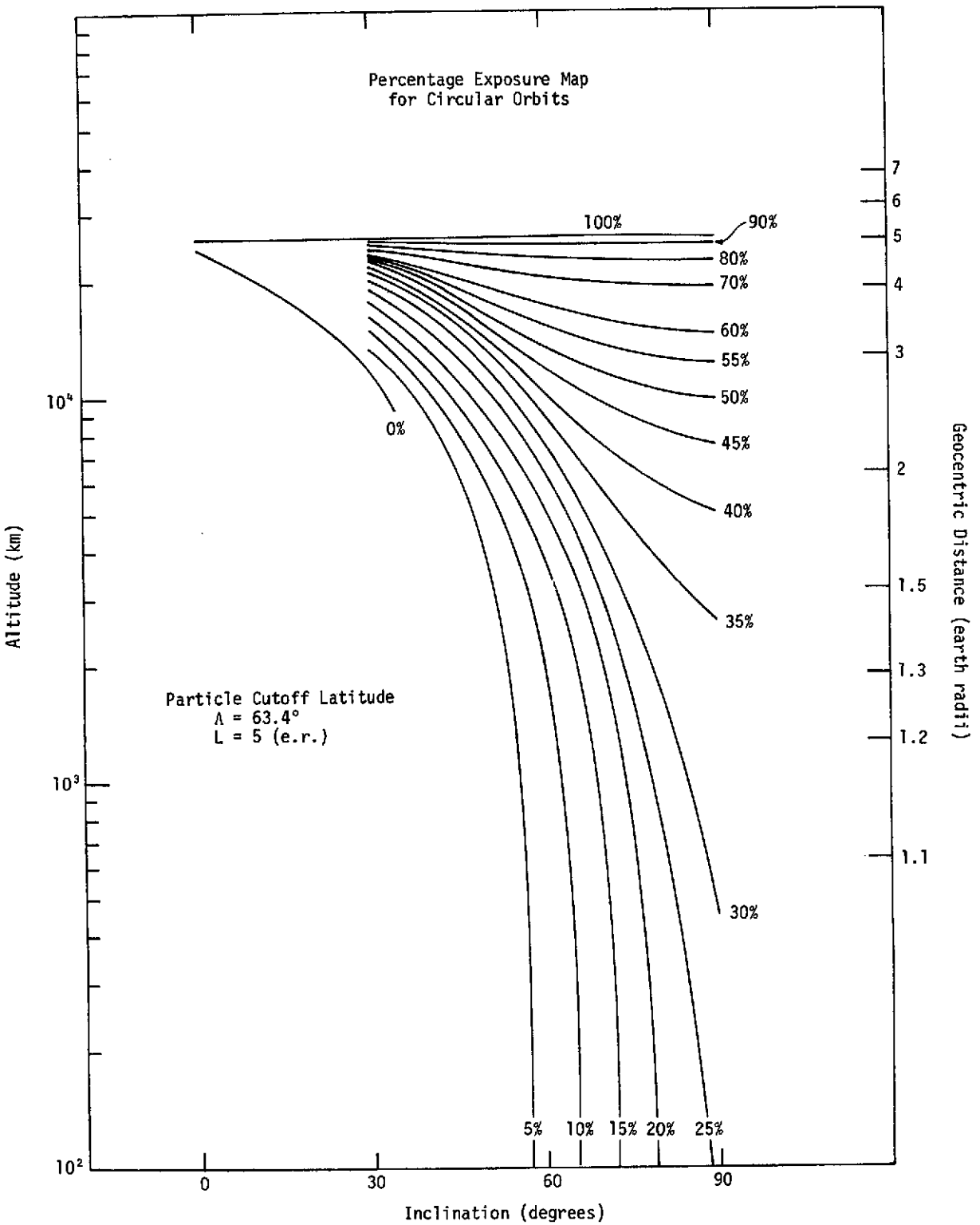
Percentage Exposure Map
for Circular Orbits
100%
90%
80%
70%
60%
55%
50%
45%
40%
35%
30%
25%
20%
15%
10%
5%
0%
Particle Cutoff Latitude
Λ = 63.4°
L = 5 (e.r.)
Altitude (km)
10⁴
10³
10²
Geocentric Distance (earth radii)
7
6
5
4
3
2
1.5
1.3
1.2
1.1
0
30
60
90
Inclination (degrees)

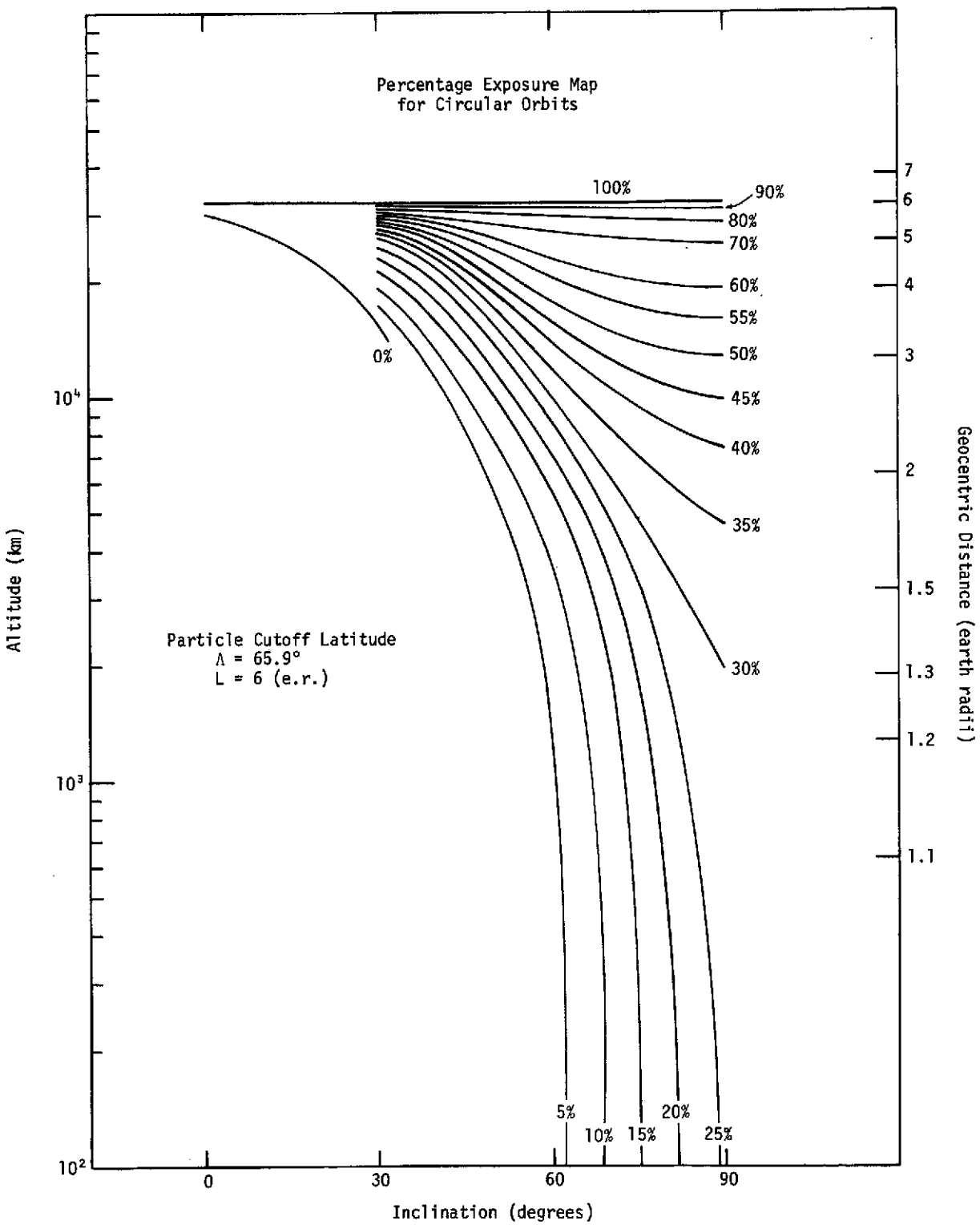
Percentage Exposure Map
for Circular Orbits
100%
90%
80%
70%
60%
55%
50%
45%
40%
35%
30%
0%
5%
10%
15%
20%
25%
Particle Cutoff Latitude
Λ = 65.9°
L = 6 (e.r.)
Altitude (km)
10⁴
10³
10²
0
30
60
90
Inclination (degrees)
Geocentric Distance (earth radii)
7
6
5
4
3
2
1.5
1.3
1.2
1.1

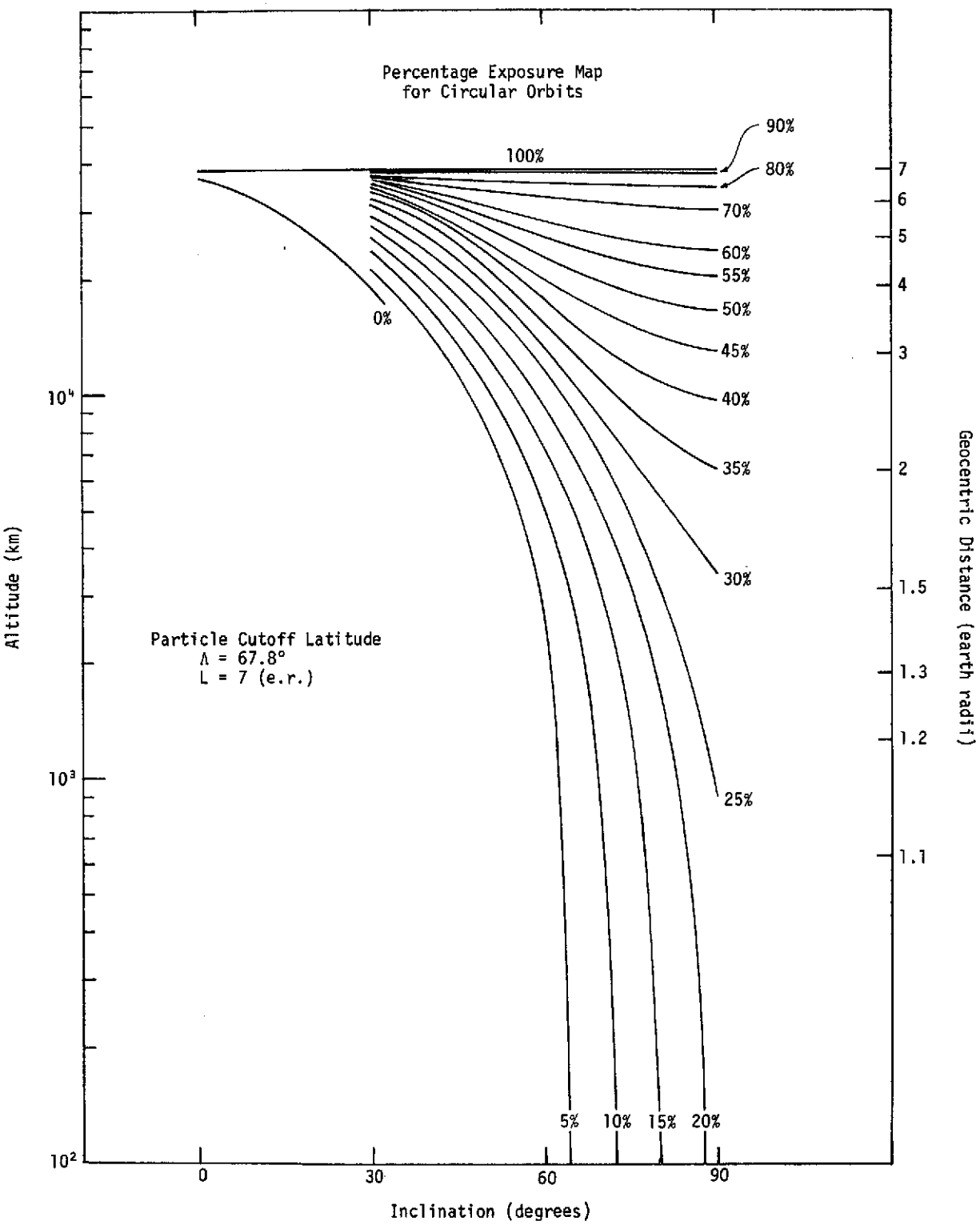
Percentage Exposure Map
for Circular Orbits
100%
90%
80%
70%
60%
55%
50%
45%
40%
35%
30%
25%
0%
5%
10%
15%
20%
Particle Cutoff Latitude
Λ = 67.8°
L = 7 (e.r.)
Altitude (km)
10⁴
10³
10²
0
30
60
90
Inclination (degrees)
7
6
5
4
3
2
1.5
1.3
1.2
1.1
Geocentric Distance (earth radii)

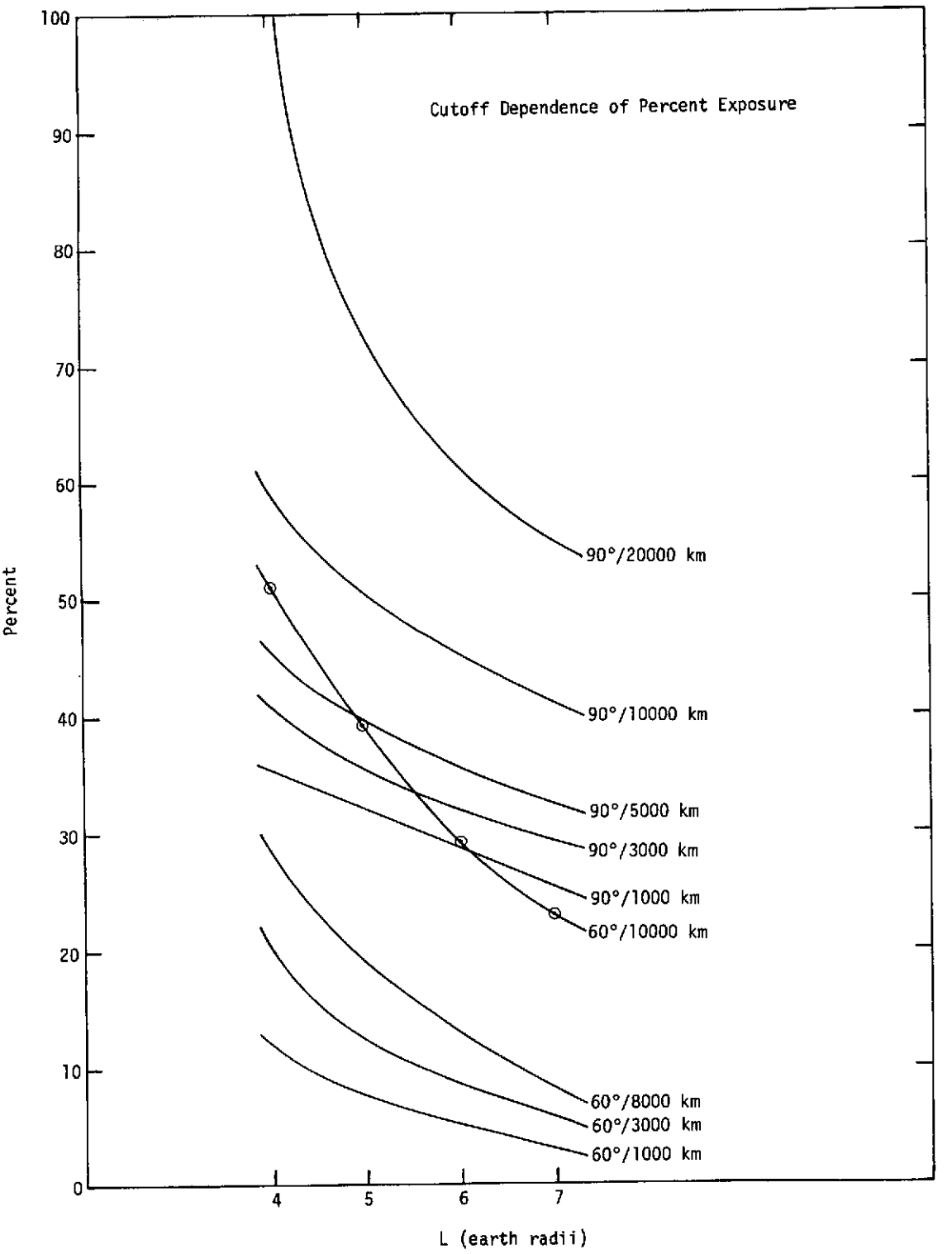
Cutoff Dependence of Percent Exposure
Percent
100
90
80
70
60
50
40
30
20
10
0
4
5
6
7
L (earth radii)
90°/20000 km
90°/10000 km
90°/5000 km
90°/3000 km
90°/1000 km
60°/10000 km
60°/8000 km
60°/3000 km
60°/1000 km

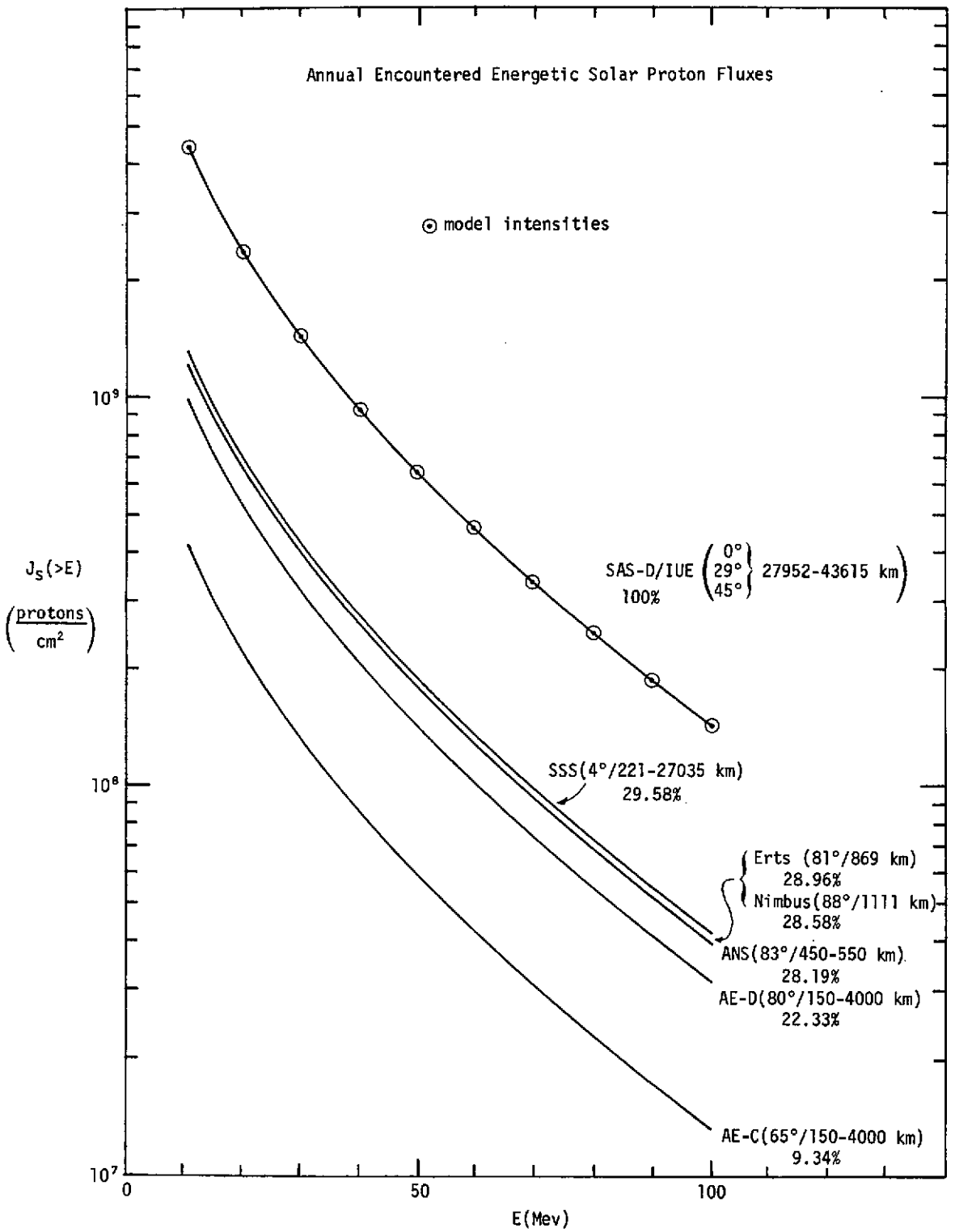
Annual Encountered Energetic Solar Proton Fluxes
⊙ model intensities
$J_S(>E)$
$\left(\frac{\text{protons}}{\text{cm}^2}\right)$
10^9
10^8
10^7
0
50
100
E(Mev)
SAS-D/IUE (0°/29°/45° 27952-43615 km) 100%
SSS(4°/221-27035 km) 29.58%
Erts (81°/869 km) 28.96%
Nimbus(88°/1111 km) 28.58%
ANS(83°/450-550 km) 28.19%
AE-D(80°/150-4000 km) 22.33%
AE-C(65°/150-4000 km) 9.34%